Dynamic Heterogeneity in Interfacial Region of Microphase-Separated Polystyrene-*block*-poly(methyl acrylate) Studied by the ESR Spin-Label Technique

Yohei Miwa,[†] Kenichi Tanida,[†] Katsuhiro Yamamoto,[†] Shigeru Okamoto,[†] Masato Sakaguchi,[‡] Masahiro Sakai,[§] Seiji Makita,[§] Shinichi Sakurai,[⊥] and Shigetaka Shimada*[,†]

Department of Materials Science & Engineering, Nagoya Institute of Technology, Gokiso-cho, Showa-ku, Nagoya 466-8555, Japan; Nagoya Keizai University, 61 Uchikubo, Inuyama 484-8503, Japan; Research Center for Molecular-Scale Nanoscience, Institute for Molecular Science, 38 Nishigo-Naka, Myodaiji, Okazaki 444-8585, Japan; and Department of Polymer Science & Engneering, Kyoto Institute of Technology, Matsugasaki, Sakyo-ku, Kyoto 606-8585, Japan

Received July 28, 2003; Revised Manuscript Received February 17, 2004

ABSTRACT: Molecular motion in an interfacial region of microdomains of polystyrene-*block*-poly(methyl acrylate) (PS-*block*-PMA) was studied by electron spin resonance (ESR) technique. The junction points between the blocks, which are located in the interfacial region, were labeled with stable nitroxide radicals. Mobility of the spin-labels reflected the dynamic environments in the interfacial region. The transition temperature of the motion of the spin-labels, $T_{5.0mT}$, at which the extreme separation width due to ^{14}N anisotropic hyperfine splitting is 5.0 mT, was estimated, and it reflects a glass transition of the region around the labels. The $T_{5.0mT}$ of the PS-*block*-PMA labeled at the junction point was almost the mean value of those of the spin-labeled PS and PMA homopolymers, and the distribution of the motional correlation times (τ_c) in the interfacial region was much broader than that in the homopolymers. These results are considered to be caused by the heterogeneous mixture of the each segment in the interfacial region at a certain length scale. The molecular weight strongly influenced the interfacial thickness and the segmental mobility and the width of the distribution of the τ_c in the interfacial region as well as on the glass transition temperatures (T_g's) of the microdomains. It was revealed that the width of the distribution of the τ_c depended on not the interfacial thickness so much as the difference between the mobilities of the block chains in the microdomains. On the other hand, extremely small effects of the overall composition and the morphology of the PS-*block*-PMA on the segmental mobility in the interfacial region were observed. From these results, it was considered that the dynamic environment in the interfacial region was strongly affected by the gradient of the segmental concentration in the interfacial region and the mobility of the block chains in the microdomains.

Introduction

Diblock copolymers with two incompatible block chains are known to form a variety of microphase-separated structures such as spheres, cylinders, lamellae, etc., depending on their compositions.[1,2] Much interest has been directed toward the nature of the domain interface because it is the important key to understanding the formation and mechanical properties of the microphase-separated polymer alloys. However, experimental measurements of characteristics of the interfacial region are difficult because of the extremely small amounts and the undefined composition of the interfacial region.

Many theories on the microphase separation are based on the concept of the three-phase system consisting of regions of pure A, pure B, and an interfacial region of mixed A and B.[3−8] Some experimental techniques have been applied to determine the interfacial thickness. Specular neutron reflectivity (SNR) measurements provide the most reliable information on the interfacial thickness of the microphase-separated structure.[9−13] Russell et al. reported that an effective thickness of the lamellar interface in polystyrene-*block*-poly(methyl methacrylate) (PS-*block*-PMMA) was evaluated to be ca. 5 nm, regardless of the molecular weight of the diblock copolymer.[9] In other ways, fluorescence decay measurement,[14−16] small-angle X-ray scattering (SAXS),[17] and differential scanning calorimetry (DSC)[18] were utilized to estimate the interfacial thickness.

In the strong segregation limit, junction points of block copolymers are concentrated in the interfacial region to minimize the surface area per chain. Matsushita et al. carried out small-angle neutron scattering (SANS) studies on polystyrene-*block*-poly(2-vinylpyridine). They revealed that the part of a block chain near the junction point was localized strongly near the interface of the lamellar microdomain, and the segmental concentration of the both components changed gradually in the interfacial region.[13,19] Russell et al. also reported a strong localization of the junction point of PS-*block*-PMMA at the lamellar interface.[20,21]

Electron spin resonance (ESR) with the spin-label technique is one of the most advantageous methods to reveal the structure and dynamic behavior of polymer chains at a particular site or in a particular region.[22−27] Recently, we studied the molecular motions at the specific sites of polystyrene-*block*-poly(methyl acrylate) (PS-*block*-PMA) with the lamellar morphology using the ESR spin-label technique.[27] In the paper, the PS-*block*-PMA was spin-labeled at the chemical junction point between the blocks, and the segmental mobility of the interfacial region was studied. The segmental mobility

[†] Nagoya Institute of Technology.
[‡] Nagoya Keizai University.
[§] Institute for Molecular Science.
[⊥] Kyoto Institute of Technology.

10.1021/ma035089i CCC: $27.50
Published on Web 04/23/2004

in the interfacial region agreed with that of the poly(styrene-*random*-methyl acrylate) with the styrene fraction of 0.5 within experimental uncertainties. This reflected the random mixture of the both components in the interfacial region. Smith et al. also studied the molecular mobility of the junction point of polystyrene-*block*-polyisoprene (PS-*block*-PI) using dynamic infrared linear dichroism spectroscopy.[28] They reported that the styrene segment near the junction point was localized near the interface, and it had rubberlike mobility even at a room temperature. Our result estimated by ESR agreed well with their result.

In the present paper, the dynamic environment in the interfacial region of microdomains was further investigated using the ESR technique. Some authors demonstrated the gradient of the segmental concentration in the interfacial region.[13,19−21] On the other hand, the dynamic heterogeneity in the interfacial region was suggested in our previous paper.[27] The relationship between the structure and the dynamic environment in the interfacial region is still unclear although the correlation is expected. Effects of the molecular weight, composition, and morphology of the PS-*block*-PMA on the dynamic environment in the interfacial region were examined. This was instructive for understanding the cause of the dynamic heterogeneity in the interfacial region. In particular, the molecular weight remarkably affected the interfacial thickness and the dynamic environment in the interfacial region. These results should clarify the relationship between the structure and the dynamic environment in the interfacial region.

Experimental Section

Materials. Styrene (ST, Extra Pure Reagent, Nacalai Tesque Co., Ltd.), methyl acrylate (MA, Extra Pure Reagent, Nacalai Tesque), *tert*-butyl acrylate (*t*BA, Extra Pure Reagent, Tokyo Chemical Co., Ltd.), and toluene (Extra Pure Reagent, Nacalai Tesque) were distilled under reduced pressure. *N*,*N*,*N*′,*N*′,*N*″-Pentamethyldiethylenetriamine (PMDETA, 99%, Aldrich Chemical Co., Ltd.), 1-phenylethyl bromide (1-PEBr, 95%, Tokyo Chemical), methyl 2-bromopropionate (MBrP, 98%, Aldrich), CuBr (98%, Aldrich), dithranol (97%, Aldrich), and 2,2,6,6-tetramethyl-4-aminopiperidine-1-oxyl (4-amino-TEMPO, 99%, Aldrich) were used as received. Tetrahydrofuran (THF), cyclohexane, and methanol were obtained from Nacalai Tesque Co., Ltd. (Extra Pure Reagent), and used without further purification.

Sample Preparation. Spin-labeled PS-*block*-PMA and PS and PMA homopolymers were synthesized by the atom transfer radical polymerization (ATRP) technique as described previously.[27] The PS-*block*-PMA was spin-labeled at the junction point, and the PS and PMA homopolymers were labeled at the inside of the chain.

Molecular weights of the PS, the PS-*block*-PMA, and the high molecular weight (more than ca. 10K) PMA were determined by gel permeation chromatography (GPC) calibrated with PS standards. Matrix-assisted laser desorption ionization, time-of-flight mass spectrometry (MALDI−TOF−MS) was used to determine the molecular weight of the low molecular weight PMA.[29,30]

The spin-labeled PS-*block*-PMA and PS and PMA homopolymers were dissolved into toluene at 5 wt %. These solutions were dried slowly at a room temperature on a Teflon plate. After the films were dried for a week, the PS-*block*-PMA and PS films were annealed in a vacuum at 393 K for 24 h. The PMA film was annealed in a vacuum at 353 K for 24 h.

Measurements. Small-angle X-ray scattering (SAXS) measurement was performed at beamline BL-9C and 15A in Photon Factory (PF) of the High Energy Accelerator Research Organization (KEK) in Tsukuba, Japan, and at beamline BL40B2 in SPring 8 in Hyogo, Japan. White radiation from the source was monochromatized using a double monochromator of Si(111) crystal to give an intense beam of $\lambda = 0.1499$ nm X-rays. The detector was a one-dimensional position-sensitive proportional counter (PSPC) located at a distance of 1.0 m (BL-9C) and 2.3 m (BL-15A) from the sample position. At BL40B2, the imaging plate (Rigaku R-AXIS) was used as a detector and located at a distance of 1.0 m. Collagen (chicken tendon) was used as a standard specimen to calibrate the SAXS detector. The experimental data were corrected for the background scattering and sample absorption.

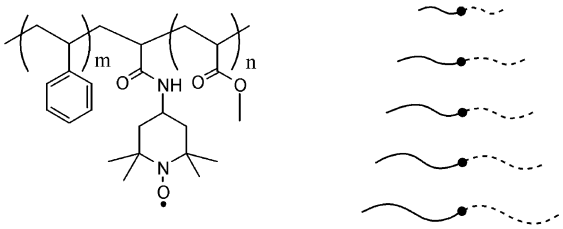

Figure 1. Chemical structures and illustrations of symmetrical PS-*block*-PMA spin-labeled at the junction point.

The M_n and M_w/M_n of the samples were determined by the GPC in THF (1 mL/min) at 313 K on four polystyrene gel columns (Tosoh TSK gel GMH (beads size is 7 μm), G4000H, G2000H, and G1000H (5 μm)) that were connected to a Tosoh CCPE (Tosoh) pump and an ERC-7522 RI refractive index detector (ERMA Inc.). The columns were calibrated against standard polystyrene (Tosoh) samples.

The MALDI−TOF−MS spectra (in linear mode) were obtained using a PreSeptive Biosystems Voyager DE-STR instrument, equipped with a N_2 laser at 337 nm to determine the M_n of PMA. Dithranol, 0.1 M in THF, doped with Na^+, was used as the matrix solution.

Nuclear magnetic resonance (NMR) was performed on a Bruker AVANCE 200 spectrometer using deuterated chloroform at 298 K with tetramethylsilane as an internal reference.

The each sample was contained in a quartz tube and the tube was depressurized to a pressure of 10^{-4} Torr and sealed before the ESR measurement. ESR spectra at 77 K and higher temperatures were observed at low microwave power level to avoid power saturation and with 100 kHz fielded modulation using JEOL JES-FE3XG and JES-RE1XG spectrometers (X band) coupled to microcomputers (NEC PC-9801). The signal of 1,1-diphenyl-2-picrylhydrazyl (DPPH) was used as a *g* tensor standard. The magnetic field was calibrated with the well-known splitting constants of Mn^{2+}.

MDSC (MDSC 2920) manufactured by TA Instruments was used. A modulation amplitude of 1.5 K and a period of 60 s were used at a heating rate of 2 K/min. The calorimeter was calibrated with an indium standard.

Results and Discussion

1. Effect of Molecular Weight on Structure and Mobility of Symmetrical PS-*block*-PMA. 1.1. Morphological Analysis of Symmetrical PS-*block*-PMA. The chemical structure and illustration of the spin-labeled PS-*block*-PMA are shown in Figure 1. The symmetrical PS-*block*-PMA's ($\phi_{PMA} \cong 0.5$) with different molecular weights were prepared. Important molecular characteristics of the samples are listed in Table 1.

The morphologies of the PS-*block*-PMA's were determined by the SAXS measurement. A plot of SAXS intensity vs scattering vector, *q*, for the PS-*block*-PMA's measured at a room temperature is shown in Figure 2. The scattering vectors of the peaks occurring at integral multiples of *q** for SM5.5, SM6.1, SM7.8, SM8.9 and SM30 obviously indicate lamellar morphologies. Here, *q** is the scattering vector of the primary scattering peak. The 2*q** diminished for SM6.1 and SM8.9 due to the disappearance rule of even number reflections for symmetric diblock copolymers. A disorder state was

Table 1. Molecular Characteristics of Samples

polymer	code	spin-label	$M_n{}^a \times 10^{-3}$	$M_w/M_n{}^a$	$M_{n,PS}{}^a \times 10^{-3}$	$\phi_{PMA}{}^b$	morphology^c	$T_{g,1}{}^d$ (K)	$T_{g,2}{}^d$ (K)	$\Delta C_{p,2}{}^d$ (J K^{-1} g^{-1})
PS-*block*-PMA	SM1.5		3.2	1.07	1.5	0.52	disorder			
PS-*block*-PMA	SM3.0	junction	6.3	1.08	3.0	0.48	lamella?^{e}	292	319	0.04
PS-*block*-PMA	SM4.5	junction	11.5	1.05	4.5	0.50	lamella?^{e}	288	323	0.08
PS-*block*-PMA	SM5.5	junction	14.3	1.08	5.5	0.54	lamella	284	327	0.08
PS-*block*-PMA	SM6.1	junction	15.6	1.05	6.1	0.51	lamella	288	338	0.09
PS-*block*-PMA	SM7.8	junction	14.9	1.04	7.8	0.52	lamella	283	336	0.09
PS-*block*-PMA	SM8.9	junction	19.0	1.08	8.9	0.49	lamella	287	344	0.10
PS-*block*-PMA	SM30	junction	56.3	1.19	30	0.51	lamella	285	367	0.20
PS	S31	inside	31.0	1.12	31.0	0			370^f	0.24^g
PMA	M29	inside	28.9	1.09		1.00		283^h		
PS-*block*-PMA	ASM30	junction	40.2	1.14	30	0.30	cylinder	285	368	
PS-*block*-PMA	ASM56	junction	65.1	1.45	30	0.56	lamella	283	369	
PS-*block*-PMA	ASM65	junction	80.3	1.25	30	0.65	lamella	284	365	

[a] By GPC columns calibrated with PS standards. [b] By ^{1}H NMR. [c] By SAXS. [d] By MDSC. [e] Predicted by symmetrical volume fraction of PS-*block*-PMA. [f] $T_{g,PS}$. [g] $\Delta C_{p,PS}$. [h] $T_{g,PMA}$.

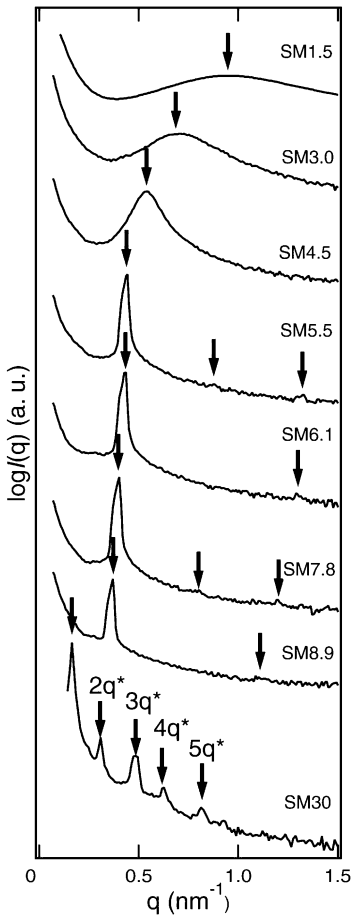

Figure 2. Intensity profile of SAXS for PS-*block*-PMA observed at room temperature.

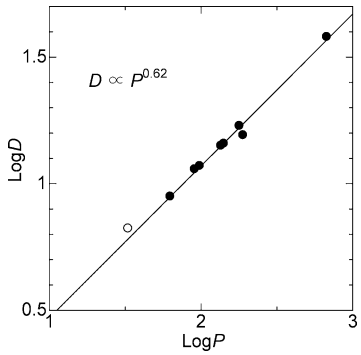

Figure 3. Double-logarithmic plot of spacing (D) and degree of polymerization (P) of PS-*block*-PMA. A power of 0.62 was obtained by best fitting using least-squares method. Spacing of SM1.5 is shown with open symbol.

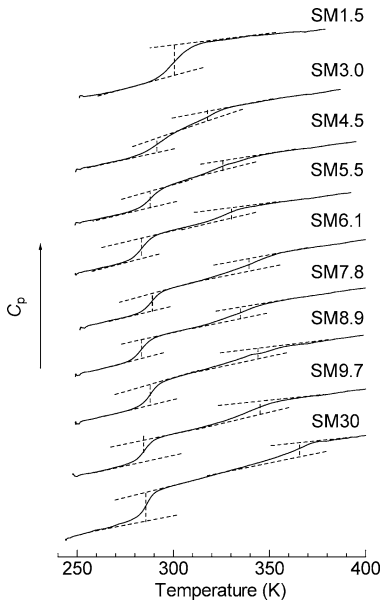

Figure 4. MDSC curves of PS-*block*-PMA's at 2 K/min with modulation amplitude of 1.5 K and 60 s period.

observed for the SM1.5, SM3.0, and SM4.5 from the SAXS measurements. However, the two distinct glass transitions were observed on the MDSC curves (see Figure 4) regardless of the observation from the broad single reflection of the SAXS for the SM3.0 and SM4.5. This might indicate that the MDSC is more sensitive than the SAXS, and the lamellar morphologies can be predicted from the symmetrical volume fraction of the SM3.0 and SM4.5 although the morphologies were unable to be determined from the scattering profile. For the SM1.5, the SAXS profile showed the broad peak, and the single glass transition was observed on the MDSC curve due to the disordered state.

The logarithm of a spacing (log D) of the PS-*block*-PMA obtained by the SAXS primary peak is plotted as a function of the logarithm of the degree of polymerization (log P) in Figure 3. The lamellar domain spacing D is proportional to the P^{α}, and the power estimated from the slope, $\alpha = 0.62$, of double logarithmic plot of D vs P is significantly larger than that ($\alpha = 0.5$) predicted for ideal Gaussian coils. On the other hand, for the strongly segregated symmetrical diblock copolymers, $\alpha = 0.67$ was obtained by experiments[9,31] and theory.[32] The $\alpha = 0.62$ of the PS-*block*-PMA is smaller than the $\alpha = 0.67$, which indicates the weaker segregation

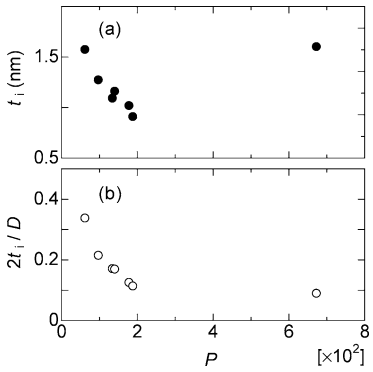

Figure 5. Width of the interface (t_i) (●) between PS and PMA lamellar microdomains and the volume fraction of specimen occupied by interface ($2t_i/D$) (○) as a function of P of PS-*block*-PMA.

between the PS and PMA than that in the strong segregation limit.

1.2. Interfacial Thickness. MDSC data also provided information on the microphase separation. MDSC curves of the PS-*block*-PMA's are shown in Figure 4. Two distinct glass transitions on the MDSC curve were exhibited for the SM3.0, SM4.5, SM5.5, SM6.1, SM7.8, SM8.9, SM9.7, and SM30, which indicated the microphase separation. On the other hand, a single glass transition brought from the disordered state was observed for the SM1.5. The increment of the heat capacity, ΔC_p, associated at the glass transition of the each phase in the PS-*block*-PMA was evaluated from the difference between the extrapolated baselines before and after the transition. The T_g was taken as the temperature corresponding to the half-height of the baseline shift. This was drawn with the broken lines in Figure 4.

The losses of the ΔC_p's at the two distinct transitions of the PS-*block*-PMA are observed, and the loss is caused by the existence of the mixed interfacial region in the microphase separation. The glass transition of the mixed interfacial region is considered to distribute over a wide range of temperature between the glass transitions of the both components because of the undefined composition in the interfacial region. On the basis of this idea, Morèse-Séguéla et al. derived the following equation[18] to determine the interfacial thickness of lamellar microdomains of PS-*block*-PI using the DSC.

$$t_i = (t_s/2)[1 - (\Delta C_{p,2}/\Delta C_{p,PS})] \quad (1)$$

Here, t_i and t_s are the thickness of the interfacial region and the PS lamellar domain, respectively. The value of the t_s was calculated from the D determined by the SAXS measurement and the volume fraction of the PS component. The values of $\Delta C_{p,2}$ associated with the PS phase of the PS-*block*-PMA are listed in Table 1. Here, the value of the $\Delta C_{p,2}$ was the increment of the heat capacity per gram of the PS component in the PS-*block*-PMA. The $\Delta C_{p,PS}$ is the increment of the heat capacity at the glass transition of the PS homopolymer. We ignored the molecular weight dependence of the ΔC_p of the PS homopolymer, which is much small for the M_n more than 3K.[33] Therefore, the $\Delta C_{p,PS}$ was given to be 0.24 J $K^{-1}g^{-1}$. The t_i was plotted against the degree of polymerization (P) of the PS-*block*-PMA in Figure 5a, and the volume fraction of the region occupied by the interface, $2t_i/D$, is plotted against the P in Figure 5b.

The t_i's were estimated to be ca. 0.5−2 nm and decreased with the increase in the P in the low molecular weight range. Morèse-Séguéla et al. also reported that the t_i of the PS-*block*-PI estimated by the DSC technique decreased with the increase in the molecular weight.[18] The t_i of the PS-*block*-PMA having the weaker segregation was larger than that of the PS-*block*-PI. On the other hand, Russell et al. estimated the t_i of symmetrical PS-*block*-PMMA to be ca. 5 nm using SNR[9] and reported that the t_i was independent of the molecular weight within experimental uncertainties in the range 30K−300K. Semenov studied the influence of the molecular weight on the t_i of strongly segregated diblock copolymers using the mean field theory and supported Russell's result.[6] In his study, the effects of chain ends and fluctuation in the position of the interface on the effective thickness of the interface were evaluated analytically, and it was demonstrated that the chain end correction for the interfacial thickness decreased with the increase in the molecular weight. On the other hand, the correction of the fluctuation was an increasing function of the molecular weight. Therefore, the interfacial thickness of the PS-*block*-PMMA was almost constant with increasing the molecular weight in the range 30K−300K. However, the chain end effect is expected to be remarkable in the range of the low molecular weight,[6] and the fluctuation effect is not taken into account for the t_i estimated by the DSC technique because it is estimated from the loss of the C_p at the glass transition. Therefore, the increase in the t_i of the PS-*block*-PMA with the decrease in the P is considered to be caused by the chain end effect suggested by Semenov.[6] The volume fraction of the region occupied by the interface, $2t_i/D$, asymptotically decreased with the increase in the P (Figure 5). This is consistent with a diblock copolymer going from the weak to strong segregation limit with increasing molecular weight.

1.3. Molecular Weight Dependence on T_g's of Microdomains. The values of $T_{g,1}$ associated with the PMA phase, together with that of $T_{g,2}$ associated with the PS phase of the PS-*block*-PMA, are listed in Table 1.

In general, T_g's are plotted against the M_n to estimate its molecular weight dependence.[34−36] However, this is probably inappropriate to compare the molecular weight dependent T_g's of different polymers. Inoue and Osaki showed via a combination of rheological and rheo-optical measurements that the "rubbery" relaxation spectrum terminates with a fastest Rouse mode that, for many polymers, corresponds well to the Kuhn length.[37] The Kuhn length, l_k, is defined as $l_k = C_\infty l$, where C_∞ and l are the characteristic ratio and a length of the average backbone bond, respectively. Therefore, the T_g was estimated as a function of the number of segments (N_s) in this work.

The $T_{g,1}$ and $T_{g,2}$ are plotted against the N_s of the PMA and PS blocks, respectively (Figure 6). The N_s was defined as the following equation:

$$N_s \equiv M_n/(C_\infty M_m) \quad (2)$$

Here, M_m is a molecular weight of the respective repeat unit, and the C_∞'s of the PMA and PS at the condition of a Gaussian coiled chain are 8 and 10, respectively.[38] The glass transition temperatures of the PMA ($T_{g,PMA}$) and PS ($T_{g,PS}$) homopolymers are also plotted against the N_s in Figure 6. In general, the number of free ends

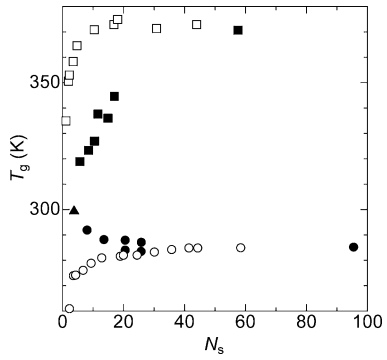

Figure 6. Plots of $T_{g,1}$ (●), $T_{g,2}$ (■), $T_{g,PMA}$ (○), and $T_{g,PS}$ (□) as a function of N_s. Single T_g of SM1.5 (▲) is also plotted.

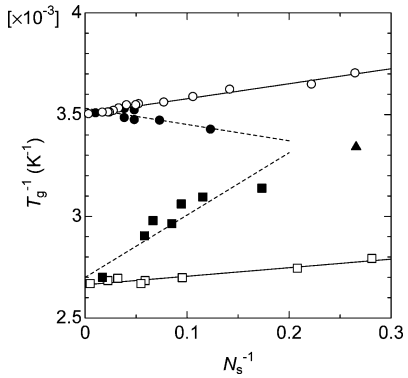

Figure 7. N_s dependence of $T_{g,1}$ (●), $T_{g,2}$ (■), $T_{g,PMA}$ (○), $T_{g,PS}$ (□), and single T_g of SM1.5 (▲). Lines were drawn by eq 3 for all data. Respective constants are listed in Table 2.

for one chain is an important factor to estimate the molecular weight dependence of the T_g. For example, the T_g of a multiarm polymer is lower than that of the linear polymer having the same molecular weight.[39] In the present work, the homopolymer has two free ends, but each block of the PS-*block*-PMA has only one free end. Therefore, twice the value of M_n of each block of the PS-*block*-PMA should be substituted in eq 2 to adjust the number of free ends with that of the homopolymer. The N_s dependence of the T_g's of the both components of the PS-*block*-PMA was much different from those of the PS and PMA homopolymers. A reduction of M_n increases the number of mobile chain ends per unit volume. Therefore, the T_g generally decreases with the reduction of the molecular weight.[26,34−36,40] However, the $T_{g,1}$ increased with the decrease in the N_s. On the other hand, the N_s dependence of the $T_{g,2}$ was stronger than that of the $T_{g,PS}$.

In Figure 7, the inverse of the $T_{g,PS}$, $T_{g,PMA}$, $T_{g,1}$, and $T_{g,2}$ is plotted as a function of reciprocal of the N_s following the Ueberreiter−Kanig equation:[36]

$$1/T_g = 1/T_{g\infty} + A/N_s \qquad (3)$$

Here, $T_{g\infty}$ is a value of the T_g at the infinite molecular weight and A is a constant. The T_g^{-1}'s showed the linear relation against the N_s^{-1}. The $T_{g\infty}$'s and A's of respective glass transitions are listed in Table 2.

It is well-known that the glass transitions of block copolymers demonstrate a different molecular weight dependence from those of homopolymers.[18,41−48] The $T_{g,1}$ and $T_{g,2}$ showed the Ueberreiter−Kanig relation as well as the $T_{g,PMA}$ and $T_{g,PS}$. However, the $T_{g,1}$ and $T_{g,2}$ demonstrated the different molecular weight dependence from those of the $T_{g,PMA}$ and $T_{g,PS}$, respectively.

Table 2. Constants of the Ueberreiter−Kanig Relation

	$T_{g\infty}$ (K)	$A \times 10^3$
$T_{g,PMA}$	285	0.7
$T_{g,PS}$	375	0.5
$T_{g,1}$	283	−0.8
$T_{g,2}$	370	3.1

This is considered to be caused by the effects of the counter components.

The A_2 (= ca. 3.1×10^{-3}) was roughly 6 times larger than the A_{PS} (= ca. 0.5×10^{-3}), which indicated the stronger molecular weight dependence of the $T_{g,2}$ than that of the $T_{g,PS}$. It is considered that the mobility of the PS component was enhanced by the mobile PMA component. On the other hand, the mobility of the PMA component was restricted by the rigid PS component. In general, the T_g reduces with a decrease in the molecular weight,[26,34−36] and the constant, A, in the Ueberreiter−Kanig equation is positive. However, the $T_{g,1}$ increased with the decrease in the N_s, and the A_1 (= -0.8×10^{-3}) was negative. In this case, the restriction on the mobility of the PMA component by the rigid PS component was considered to be stronger than the relaxing effect by the mobile PMA chain ends with the reduction of the molecular weight of the PMA block. As shown in Figure 3, the lamellar spacing decreased with the reduction of the molecular weight. This implies that the ratio of the interfacial area per unit volume of the PS-*block*-PMA, in other words, the effect by the counter components, increases with the reduction of the molecular weight. In fact, the $T_{g,1}$ of the SM3.0 was the highest in those copolymers, and the $T_{g\infty,1}$ (= ca. 283 K) and $T_{g\infty,2}$ (= ca. 370 K) roughly agreed with the $T_{g\infty,PMA}$ (= ca. 285 K) and $T_{g\infty,PS}$ (= ca. 375 K), respectively. This result indicates that the influence by the counter components is negligible at the infinite molecular weight. When the N_s^{-1} is larger than the cross point of the extrapolated lines of the Ueberreiter−Kanig relations of the $T_{g,1}$ and $T_{g,2}$, phase separation is unexpected. In fact, the single glass transition come from the disordered state was observed for the SM1.5, as shown in Figure 4. Morèse-Séguéla et al. also reported the same behavior on the T_g's of rigid and soft components of PS-*block*-PI.[18]

1.4. Molecular Motion of Junction Point between PS and PMA Blocks in the Interfacial Region. Broad Distribution of τ_c in the Interfacial Region. Temperature-dependent ESR spectra of the S31, M29, SM3.0, SM8.9, and SM30 are compared with each other in the temperature range 77−453 K in Figure 8. The temperature dependence of the spectra is due to the change of the motional correlation time τ_c. The main triplet spectrum was induced by hyperfine coupling with a nitrogen nucleus. The outermost splitting of the triplet spectrum narrows with an increase in mobility of the radicals because of motional averaging of the anisotropic interaction between an electron and a nucleus. The complete averaging gives rise to the isotropic narrowed spectrum.

In contrast with a single spectral component of the temperature-dependent ESR spectra of the S31, M29, and SM3.0, two spectral components, a "first" and a "slow" component, were remarkably observed for the SM8.9 and SM30. The slow component with large outermost splitting width and the fast component with small outermost splitting width and narrow line width are considered be attributed to radicals in rigid and mobile regions, respectively. In general, the two spectral

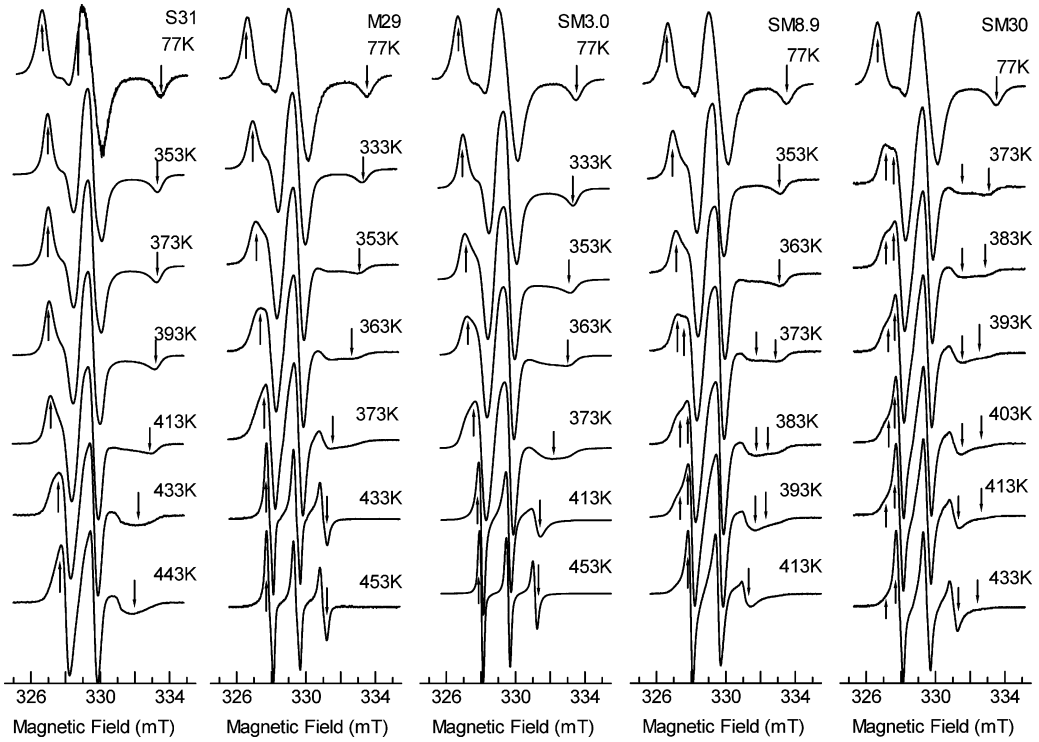

Figure 8. Temperature-dependent ESR spectra of S31, M29, SM3.0, SM8.9, and SM30. Sample codes are shown in the figure. The separation between arrows shows the extreme separation width.

components are observed for crystalline polymers, polymer blends, block and graft copolymers, etc.,[25,27,33,49−54] and those are not observed for amorphous homopolymers[26] and random copolymers.[27] Some ESR spin-label studies suggested that the scale of the region explored by the label is of the order of ca. 5−10 monomeric units, which depends on the structure of polymers.[25,26,40] Therefore, it is considered that the two spectral components are the reflection of a broad distribution of the τ_c arising from heterogeneous structures over the higher order of the scale than that explored by the spin-labels.[55,56] For instance, the heterogeneity of the segmental concentration, the segmental density, and the free volume around the spin-labels can originate the distribution of the τ_c.

In the present work, the spin-labels at the junction points of the PS-*block*-PMA are considered to be concentrated in the interfacial region. In fact, some authors demonstrated that the junction points of diblock copolymers strongly localized at the interface,[13,19−21] and the mobility of the spin-labels also suggested that the labels were concentrated in the interfacial region. Two characteristic temperatures, T_f and T_s, were estimated for the PS-*block*-PMA labeled at the junction point in our previous paper.[27] Here, the T_f was where the fast component appeared, while the T_s was where the slow component completely disappeared.[57] The T_s and T_f roughly agreed with transition temperatures, $T_{5.0mT}$'s (see below), of the PS and PMA homopolymers, respectively. From these results, the heterogeneous structure (the concentration heterogeneity of the each segment) in the interfacial region is considered to cause two spectral components of the PS-*block*-PMA labeled at the junction point.

Here, one question is arising. Does the τ_c have a broad continuous distribution or a bimodal distribution in the interfacial region? As Cameron et al. pointed out, the two spectral components are brought from not only the bimodal distribution but also the broad continuous distribution of the τ_c around the labels.[55] Many experiments[9,12,13,21,22] and theories[7,32] suggested that the gradient of the each segmental concentration in the interfacial region was continuous, and the mobility of the spin-labels is expected to be affected by the local segmental concentration around the labels in the interfacial region. In fact, we previously demonstrated that the mobility of the spin-labels was dependent on the composition in miscible random copolymhers.[27] Therefore, we consider that the distribution of the τ_c in the interfacial region might be continuous.[55]

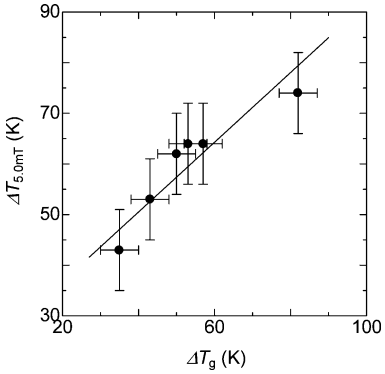

Figure 9. Relationship between $\Delta T_{5.0mT}$ (= T_s − T_f) and ΔT_g (= T_2 − T_1).

The relation of $\Delta T_{5.0mT}$ (the difference between the T_f and the T_s) to ΔT_g (the difference between the $T_{g,1}$ and $T_{g,2}$) of SM samples is shown in Figure 9. The width of the distribution of the τ_c in the interfacial region was considered to relate to $\Delta T_{5.0mT}$, and it increased with the increase in the difference between the mobilities of the block chains in the microdomains. For the SM3.0, the single spectral component was observed as well as the S31 and M29. The single spectral component is the reflection of the relatively narrow distribution of the τ_c

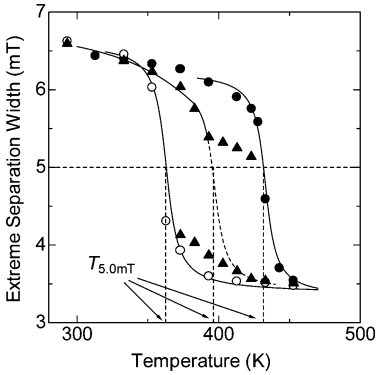

Figure 10. Temperature dependence of extreme separation width. $T_{5.0mT}$ are 431, 367, and 398 K for S31 (●), M29 (○), and SM30 (▲), respectively.

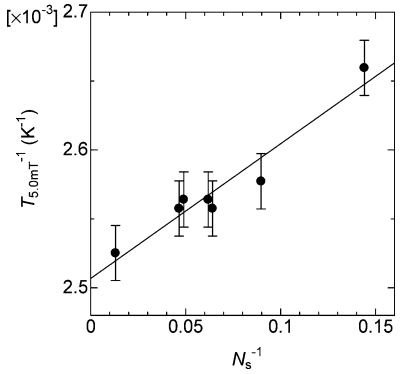

Figure 11. Plot of $T_{5.0mT}^{-1}$ of PS-*block*-PMA labeled at junction point vs N_s^{-1}. Line was drawn by eq 3.

around the spin-labels. Although the SM3.0 was spin-labeled at the junction point, the T_g's of the PS and PMA microdomains were considerably close to each other (see Figure 4). Therefore, it was considered that the distribution of the τ_c in the interfacial region of the SM3.0 was narrow, and the single spectral component was observed. On the other hand, as shown in Figure 5, the interfacial thickness increased with the reduction of the molecular weight. One expects that the dynamic heterogeneity is enhanced by the increase in the thickness of the interfacial region. However, the result in Figure 9 indicated that the distribution of the τ_c in the interfacial region decreased with the reduction of the molecular weight. The dynamic heterogeneity in the interfacial region looks not to be as a function of the interfacial thickness. In this case, it is considered that the difference between the segmental mobility's of the block chains in the microdomain had a larger influence than the interfacial thickness on the dynamic heterogeneity in the interfacial region.

Transition Temperature. A temperature dependence of the extreme separation width between the arrows in Figure 8 is shown in Figure 10. The extreme separation width gradually decreases and steeply drops with an increase in temperature. The steep drop is caused by a micro-Brownian-type molecular motion.[26,58−60] A transition temperature of molecular motion, $T_{5.0mT}$, at which the extreme separation width is equal to 5.0 mT was estimated. The $T_{5.0mT}$'s of the S31 and M29 are 431 and 367 K, respectively. The SM30 showed the two spectral components due to the broad distribution of the τ_c. Therefore, the $T_{5.0mT}$ of the SM30 was defined to be the temperature where the extreme separation width of the major spectral component was equal to 5.0 mT. It is shown in Figure 10 and estimated to be 398 K. The $T_{5.0mT}$ includes ±2.5 K of experimental uncertainties.

In general, the $T_{5.0mT}$ appears at higher than a glass transition temperature, T_g, obtained by the DSC because of the higher frequency of the ESR.[26,58−60] In our previous paper, we compared the $T_{5.0mT}$ with the T_g in detail for the PS and PMMA homopolymers.[26,40] The $T_{5.0mT}$ reduced to the T_g using the time−temperature superposition of the WLF equation.[61] Moreover, the $T_{5.0mT}$'s showed the molecular weight dependence as well as the T_g's of the PS and PMMA. These results demonstrated that the $T_{5.0mT}$ reflected the glass transition of the region around the spin-labels at the frequency of the ESR. Note that the spin-labels are covalently connected to a side group tethered to the main chain. However, the cooperative motion with neighboring segments is necessary to undergo a rotational relaxation at the glass transition,[62] and the size of the spin-label was roughly comparable to those of the styrene and methyl acrylate monomers. Therefore, the spin-labels might move cooperatively with repeat units. As a consequence, it is considered that the motion of the spin-labels reflected the glass transition.

The $T_{5.0mT}$ of the SM30 was almost the mean value of those of the S31 and M29, and our previous paper reported that the $T_{5.0mT}$ of the SM30 was comparable to that of the spin-labeled poly(styrene-*random*-methyl acrylate) (poly(ST-*random*-MA)) with the styrene fraction of 0.5. These results are suggestive for understanding the dynamic environment in the interfacial region. The structural analyses by other authors suggested that the both components were mixing in the interfacial region. Hence, we also consider that the chain in the interfacial region might be as mobile as that in miscible polymer blends.[9,12,13,21,22]

The segmental dynamics of miscible polymer blends have been the focus of recent research. The two constituents sometimes appear to experience different average dynamic environments even in the macroscopically miscible blends. It has been suggested that these results can be attributed to concentration fluctuations coupled to chain connectivity effects.[63] Lodge and McLeish showed that the self-concentration of each segment in the effective volume brought from the chain connectivity was important for the local dynamics of miscible polymer blends.[64] In the case of the junction point, the self-concentration effect of the each segment brought from the chain connectivity around the junction point is considered to be comparable to each other. Therefore, the estimated average mobility of the junction in the interfacial region was roughly mean between those of the PS and PMA. However, in contrast with the single spectral components of the spin-labeled poly(ST-*random*-MA), the PS-*block*-PMA labeled at the junction point obviously showed the two spectral components which reflected the concentration heterogeneity in the interfacial region. In other words, the mobility of the junctions in the interfacial region was strongly affected by the segmental concentration and its heterogeneity in the interfacial region.

Molecular Weight Dependence on Mobility of Junction Points in the Interfacial Region. The inverse of the $T_{5.0mT}$ was plotted as a function of the reciprocal of the N_s following the Ueberreiter−Kanig relation in Figure 11. Here, the N_s for the $T_{5.0mT}$ was defined as the sum of the N_s's of the PS and PMA blocks.

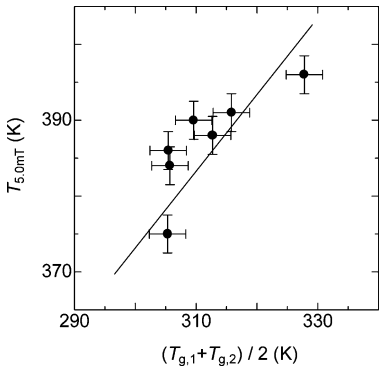

Figure 12. Relationship between $T_{5.0mT}$ of PS-*block*-PMA labeled at junction point and $(T_1 + T_2)/2$. The slope of line is unity.

The linear relation of the $T_{5.0mT}{}^{-1}$ vs $N_s{}^{-1}$ was observed as well as the other T_g's. The $T_{5.0mT\infty}$ and A were ca. 399 K and 1.0×10^{-3}, respectively. This indicates that the mobility of the junction points in the interfacial region depended on the M_n, in other words, the chain ends fraction of the PS-*block*-PMA. In general, the decrease in the T_g with the reduction of the M_n is interpreted in terms of the increase in the mobile chain end fraction. However, as Matsushita et al. and Russell et al. demonstrated, the free chain ends of the diblock copolymer with the lamellar morphology were concentrated on the center of the microdomain with a fairly wide distribution, and the population of the chain ends at the interface was small. Therefore, the influence of the mobile chain ends on the mobility in the interfacial region is expected to be negligible.

As described above, the mobility of the block chains in the microdomains has influenced remarkably that in the interfacial region. Therefore, the $T_{5.0mT}$ was plotted against the mean mobility of the microdomains assumed to be $(T_{g,1} + T_{g,2})/2$ in Figure 12. The linear relation between the $T_{5.0mT}$ and the $(T_{g,1} + T_{g,2})/2$ was obtained, and the slope was close to be unity within the experimental uncertainties. This result suggested that segmental mobility in the interfacial region was comparable to the mean mobility of the block chains in the microdomains, and the molecular weight dependence on the segmental mobility in the interfacial region was interpreted in terms of the segmental mobility of the block chains in the microdomains.

2. Influence of Composition and Morphology of PS-*block*-PMA on Mobility in the Interfacial Region. 2.1. Morphological Analysis. Asymmetrical PS-*block*-PMA's were prepared via the ATRP technique, and the molecular characteristics of the samples are listed in Table 1.

The morphologies of the PS-*block*-PMA's were determined by the SAXS. The SAXS profiles measured at a room temperature are shown in Figure 13. The morphologies of the samples were indicated by multiple reflections. The scattering vectors of the peaks occurring at integral multiples of q^* indicate the lamellar morphologies for the ASM56 and the ASM65. For the ASM30, the q_n/q^* ratio of 1, $\sqrt{3}$, $\sqrt{4}$, and $\sqrt{7}$ indicates the hexagonal cylinder morphologies.

2.2. Mobility of Junction Points in the Interfacial Region. Effects of the composition and the morphology of the PS-*block*-PMA on the mobility of the junction points are studied. Curved interfaces are expected for the sphere and cylinder morphologies in contrast with a flat interface of the lamella. It is known

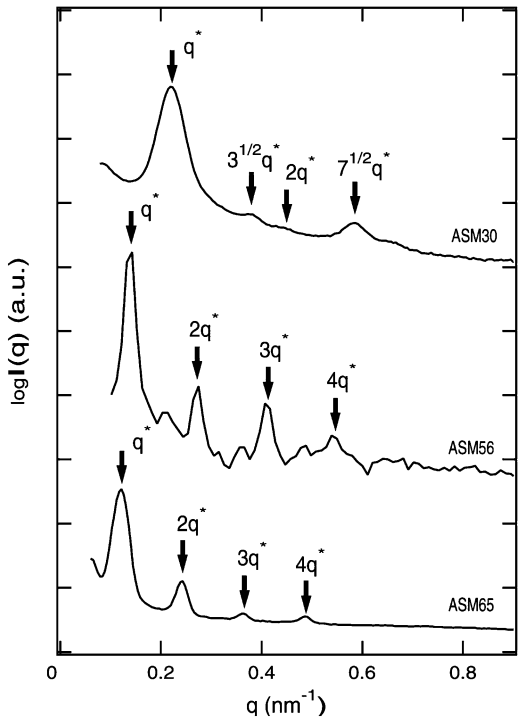

Figure 13. SAXS intensity of asymmetrical PS-*block*-PMA as a function of q at room temperature.

that the lamellar morphology brings the chain conformation relatively extended to the perpendicular direction against the interface.[65] In fact, as shown in Figure 3, the $\alpha = 0.62$ estimated from the double-logarithmic plot of D vs P for the symmetrical PS-*block*-PMA with lamella morphology was significantly larger than that ($\alpha = 0.5$) predicted for ideal Gaussian coils. This implied that the relatively extended conformation of the PS-*block*-PMA to the perpendicular direction against the interface. On the other hand, smaller α's than that of the lamella are expected for the sphere and cylinder morphologies because the extension on the chain conformation might be reduced by the curvature of the interface. Namely, the different chain conformations are expected to be induced by the different morphologies.

Temperature-dependent ESR spectra of the ASM30, ASM56, and ASM65 are shown in Figure 14. Two spectral components were observed for the all samples. This is considered to reflect the heterogeneity of the segmental concentration in the interfacial region as mentioned above.

The $T_{5.0mT}$'s of the ASM30, ASM56, and ASM65 were compared with that of the SM30 to consider the effects of the composition and morphology on the mobility of the junction points. From the result of the above section, the molecular weight effect on the mobility of the junctions can be ignored for these samples because those molecular weights are sufficiently large. The $T_{5.0mT}$'s of the ASM30, ASM56, and ASM65 were estimated to be 397, 399, and 396 K, respectively. These values agreed well with the $T_{5.0mT}$ of the SM30 (=398 K). This result obviously demonstrated that effects of the composition and morphology of the PS-*block*-PMA on the segmental mobility in the interfacial region were extremely small. As described above, the region explored by the label is considered to be ca. 5−10 monomeric units around the label.[25,26,40] The scale of the morphology change and the increase in the D is much larger than that of the region explored by the spin-labels. This is considered to be the

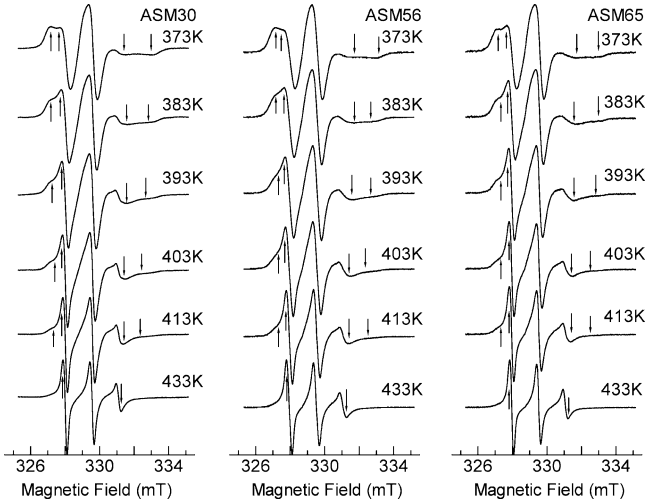

Figure 14. Temperature-dependent ESR spectra of asymmetrical PS-*block*-PMA labeled at the junction point. Sample codes are shown in the figure.

cause of this result. Moreover, the $T_{g,1}$'s and $T_{g,2}$'s of the ASM30, ASM56, and ASM65 were almost equal to those of the SM30 (Table 1). Therefore, the mobility in the interfacial region of the ASM30, ASM56, ASM65, and SM30 almost agreed with each other. As a result, it was revealed that the overall composition and morphology of the PS-*block*-PMA had extremely small effects on the segmental mobility in the interfacial region.

Conclusion

The dynamic heterogeneities in the interfacial region of the microphase-separated PS-*block*-PMA were revealed by the ESR spin-label technique. The $T_{5.0mT}$ of the PS-*block*-PMA labeled at the junction point was roughly mean of those of the spin-labeled PS and PMA homopolymers. On the other hand, the broad distribution of the τ_c in the interfacial region was observed. These results reflected the heterogeneous mixture of the both components in the interfacial region. It was revealed that the segmental mobility and the distribution of the τ_c in the interfacial region were strongly affected by the T_g's of the microdomains. On the other hand, extremely small effects of the interfacial thickness, the overall composition, and morphology of the PS-*block*-PMA on the segmental mobility in the interfacial region were observed. This result implied that the scale of the segmental motion explored by the spin-labels was much smaller than those of the interfacial thickness, the overall composition, and the morphology of the PS-*block*-PMA, and the effects of the interfacial thickness, the overall composition, and the morphology on the segmental concentration in the interfacial region were negligible. In conclusion, it is considered that the dynamic heterogeneities in the interfacial region were due to the gradient of the segmental concentration in the interfacial region, and the dynamic environment in the interfacial region was strongly influenced by the mobility of the block chains in the microdomains.

Acknowledgment. Thanks are due to the Research Center for Molecular-Scale Nanoscience, the Institute for Molecular Science, for assistance in obtaining the MDSC and the MALDI−TOF−MS data. The SAXS measurement was performed under approval of the Photon Factory Program Advisory Committee (Proposal No. 2001G269, 2001G275, and 2003G275) and SPring8 Program Advisory Committee (Proposal No. 2003A0297-NL2-np, 2003A0314-NL2-np, and 2003B0151-NL2b-np). The financial support of a part of this project is by a grant from the NITECH 21st Century COE Program "World Ceramics Center for Environmental Harmony". We thank Prof. K. Sakurai and Dr. I. Akiba of The University of Kitakyushu for fruitful discussions.

References and Notes

(1) Hasegawa, H.; Tanaka, H.; Yamasaki, K.; Hashimoto, T. *Macromolecules* **1987**, *20*, 1651.
(2) Bates, F. S. *Science* **1991**, *151*, 898.
(3) Leary, D. F.; Williams, M. C. *J. Polym. Sci., Polym. Phys. Ed.* **1973**, *11*, 345.
(4) Meier, D. J. *Polym. Prepr. (Am. Chem. Soc., Div. Polym. Chem.)* **1974**, *15*, 171.
(5) Helfand, E. *Macromolecules* **1975**, *8*, 552.
(6) Semenov, A. N. *Macromolecules* **1993**, *26*, 6617.
(7) Helfand, E.; Wasserman, Z. R. *Macromolecules* **1976**, *9*, 879.
(8) Helfand, E.; Bhattacharjee, S. M.; Fredrickson, G. H. *J. Chem. Phys.* **1989**, *91*, 7200.
(9) Anastasiadis, S. H.; Russell, T. P.; Satija, S. K.; Majkrzak, C. F. *J. Chem. Phys.* **1990**, *92*, 5677.
(10) Russell, T. P.; Menelle, A.; Hamilton, W. A.; Smith, G. S.; Satija, S. K.; Majkrzak, C. F. *Macromolecules* **1991**, *24*, 5721.
(11) Anastasiadis, S. H.; Retsos, H.; Toprakcioglu, C.; Menelle, A.; Hadziioannou, G. *Macromolecules* **1998**, *31*, 6600.
(12) Bucknall, D. G.; Fernández, M. L.; Higgins, J. S. *Faraday Discuss.* **1994**, *98*, 19.
(13) Torikai, N.; Noda, I.; Krrarim, A.; Satija, S. K.; Han, C. C.; Matsushita, Y.; Kawakatsu, T. *Macromolecules* **1997**, *30*, 2907.
(14) Rharbi, Y.; Winnik, M. A. *Macromolecules* **2001**, *34*, 5238.
(15) Ni, S.; Zhang, P.; Wang, Y.; Winnik, M. A. *Macromolecules* **1994**, *27*, 5742.
(16) Tcherkasskaya, O.; Ni, S.; Winnik, M. A. *Macromolecules* **1996**, *29*, 610.
(17) Hashimoto, T.; Todo, H.; Itoi, H.; Kawai, H. *Macromolecules* **1977**, *10*, 377.
(18) Morèse-Séguéla, B.; St-Jacques, M.; Renaud, J. M.; Prud'homme, J. *Macromolecules* **1980**, *13*, 100.
(19) Torikai, N.; Matsushita, Y.; Noda, I.; Karim, A.; Satija, S. K.; Han, C. C. *Physica B* **1995**, *213 & 214*, 694.
(20) Mayes, A. M.; Johnson, R. D.; Russell, T. P.; Smith, S. D.; Satija, S. K.; Majkrzak, C. F. *Macromolecules* **1993**, *26*, 1047.
(21) Shull, K. R.; Mayes, A. M.; Russell, T. P. *Macromolecules* **1993**, *26*, 3929.
(22) Sakaguchi, M.; Yamaguchi, T.; Shimada, S.; Hori, Y. *Macromolecules* **1993**, *26*, 2612.
(23) Shimada, S.; Sugimoto, A.; Kawaguchi, M. *Polymer* **1997**, *38*, 2251.
(24) Shimada, S.; Watanabe, T. *Polymer* **1998**, *39*, 1711.
(25) Schlick, S.; Harvey, R. D.; Alonso-Amigo, M. G.; Klempner, D. *Macromolecules* **1989**, *22*, 822.
(26) Miwa, Y.; Tanase, T.; Yamamoto, K.; Sakaguchi, M.; Sakai, M.; Shimada, S. *Macromolecules* **2003**, *36*, 3235.
(27) Miwa, Y.; Yamamoto, K.; Sakaguchi, M.; Sakai, M.; Tanida, K.; Hara, S.; Okamoto, S.; Shimada, S. *Macromolecules* **2004**, *37*, 831.
(28) Smith, S. D.; Noda, I.; Marcott, C.; Dowrey, A. E. *Polymer Solutuins, Blends and Interfaces*; Elsevier Science Publishers, B.V.: Amsterdam, 1992.
(29) Nonaka, H.; Ouchi, M.; Kamigaito, M.; Sawamoto, M. *Macromolecules* **2001**, *34*, 2083.
(30) Cho, D.; Park, S.; Kwon, K.; Chang, T.; Roovers, J. *Macromolecules* **2001**, *34*, 7570.
(31) Matsushita, Y.; Mori, K.; Saguchi, R.; Nakao, Y.; Noda, I.; Nagasawa, M. *Macromolecules* **1990**, *23*, 4313.
(32) Melenkevitz, J.; Muthukumar, M. *Macromolecules* **1991**, *24*, 4199.
(33) Aras, L.; Richardson, M. J. *Polymer* **1989**, *30*, 2246.
(34) Fox, T. G.; Flory, P. J. *J. Appl. Phys.* **1950**, *21*, 581.
(35) Beevers, R. B.; White, E. F. T. *Trans. Faraday Soc.* **1960**, *56*, 117.
(36) Ueberreiter, K.; Kanig, G. *J. Colloid Sci.* **1952**, *7*, 569.
(37) Inoue, T.; Osaki, K. *Macromolecules* **1996**, *29*, 1595.
(38) *Polymer Handbook*, 3rd ed.; John Wiley & Sons: New York, 1989.
(39) Roovers, J. E. L.; Toporowski, P. M. *J. Appl. Polym. Sci.* **1974**, *18*, 1685.

(40) Miwa, Y.; Yamamoto, K.; Sakaguchi, M.; Sakai, M.; Makita, S.; Shimada, S. *J. Phys. Chem.*, to be submitted.
(41) Krause, S.; Iskandar, M.; Iqbal, M. *Macromolecules* **1982**, *15*, 105.
(42) Krause, S.; Iskandar, M. *Adv. Chem. Ser.* **1979**, *176*, 205.
(43) Gaur, U.; Wunderlich, B. *Macromolecules* **1980**, *13*, 1618.
(44) Toporowski, P. M.; Roovers, J. E. L. *J. Polym. Sci., Polym. Chem. Ed.* **1976**, *14*, 2233.
(45) Kraus, G.; Rollmann, K. W. *J. Polym. Sci., Polym. Phys. Ed.* **1976**, *14*, 1133.
(46) Mohammady, S. Z.; Mansour, A. A.; Knoll, K.; Stoll, B. *Polymer* **2002**, *43*, 2467.
(47) Kraus, G.; Childers, C. W.; Gruver, J. T. *J. Appl. Polym. Sci.* **1967**, *11*, 1581.
(48) Lu, Z.; Krause, S. *Macromolecules* **1982**, *15*, 112.
(49) Cameron, G. G.; Qureshi, M. Y.; Tavern, S. C. *Eur. Polym. J.* **1996**, *32*, 587.
(50) Brown, I. M. *Macromolecules* **1981**, *14*, 801.
(51) Shimada, S.; Kozakai, M.; Yamamoto, K. *Polymer* **1998**, *32*, 6013.
(52) Varghese, B.; Schlick, S. *J. Polym. Sci., Part B: Polym. Phys.* **2002**, *40*, 415.
(53) Cameron, G. G.; Qureshi, M. Y.; Stewart, D.; Buscall, R.; Nemcek, J. *Polymer* **1995**, *36*, 3071.
(54) Cameron, G. G.; Stewart, D. *Polymer* **1996**, *37*, 5329.
(55) Cameron, G. G.; Miles, I. S.; Bullock, A. T. *Br. Polym. J.* **1987**, *19*, 129.
(56) Brown, I. M.; Sandreczki, T. C. *Macromolecules* **1985**, *18*, 2702.
(57) Yamamoto, K.; Shimada, S.; Tsujita, Y.; Sakaguchi, M. *Macromolecules* **1997**, *30*, 1776.
(58) Shimada, S.; Kashima, K. *Polym. J.* **1996**, *28*, 690.
(59) Sohma, J.; Sakaguchi, M. *Adv. Polym. Sci.* **1978**, *20*, 109.
(60) Kusumoto, N.; Sano, S.; Zaitsu, N.; Motozato, Y. *Polymer* **1976**, *17*, 448.
(61) Williams, M. L.; Landel, R. F.; Ferry, J. D. *J. Am. Chem. Soc.* **1995**, *77*, 3701.
(62) Matsuoka, S.; Quan, X. *Macromolecules* **1991**, *24*, 2770.
(63) Kant, R.; Kumar, S. K.; Colby, R. H. *Macromolecules* **2003**, *36*, 10087.
(64) Lodge, T. P.; McLeish, T. C. *Macromolecules* **2000**, *33*, 5278.
(65) Matsushita, Y.; Mori, K.; Saguchi, R.; Noda, I.; Nagasawa, M.; Chang, T.; Glinka, C. J.; Han, C. C. *Macromolecules* **1990**, *23*, 4387.

MA035089I